Structural and spectroscopic study of adsorption of anthracene on silver

ARTICLE *in* JOURNAL OF MOLECULAR STRUCTURE · JUNE 2015

Impact Factor: 1.6 · DOI: 10.1016/j.molstruc.2014.09.022

3 AUTHORS, INCLUDING:

Mahalingam Umadevi

Mother Teresa Women's University

99 PUBLICATIONS **747** CITATIONS

SEE PROFILE

Beulah JM Rajkumar

Lady Doak College

20 PUBLICATIONS **244** CITATIONS

SEE PROFILE

Journal of Molecular Structure 1079 (2015) 155–162

Contents lists available at ScienceDirect

Journal of Molecular Structure

journal homepage: www.elsevier.com/locate/molstruc

Structural and spectroscopic study of adsorption of naphthalene on silver

T.N. Rekha [a], M. Umadevi [b], Beulah J.M. Rajkumar [a,*]

[a] PG & Research Department of Physics, Lady Doak College, Madurai 625002, India
[b] Department of Physics, Mother Teresa Women's University, Kodaikanal 624101, India

HIGHLIGHTS

- Adsorption characteristics of naphthalene on silver documented using DFT and SERS.
- Binding of π electrons of naphthalene with valence electrons of silver established.
- SERS studies infer tilted orientation of naphthalene on the silver surface.
- Lower bandgap of naphthalene on adsorption and localization in electron density.
- Utility in the design of electro active organic molecular devices.

GRAPHICAL ABSTRACT

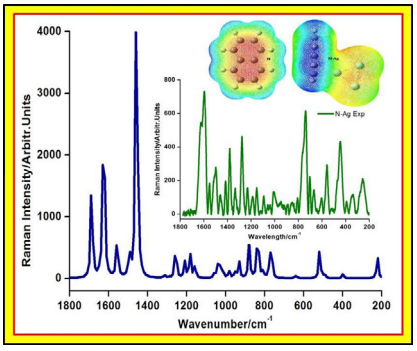

ARTICLE INFO

Article history:
Received 30 July 2014
Received in revised form 6 September 2014
Accepted 8 September 2014
Available online 16 September 2014

Keywords:
TDDFT
Naphthalene
NBO analysis
Intramolecular charge transfer
SERS

ABSTRACT

Adsorption characteristics of naphthalene on silver are investigated using methods based on Density Functional Theory (DFT) and Surface Enhanced Raman Spectroscopy (SERS). Variations in bond angles and dihedral angles of the optimized geometry of naphthalene after adsorption on silver indicate distorted hexagonal structure of the ring nearer to Ag atoms and deviations in co-planarity of carbon atoms. Theoretical computations establish binding interactions through π electrons as natural bond orbital analysis confirms intramolecular charge transfers originating from the orbital overlap between π(C—C) to π^*(C—C) and π(C—C) to σ^*(Ag—Ag) orbitals. Higher polarization values resulting from charge transfers on adsorption, indicated by DFT calculations, account for Raman enhancement of selective vibrational modes and band shifts. Silver nanoparticles (Ag NPs) were prepared using solution combustion method and were characterized by X-ray diffraction (XRD) and High Resolution Transmission Electron Microscopy (HRTEM). Surface plasmon resonance peak observed around 412 nm in the optical absorption spectrum of Ag NPs after adsorption of naphthalene is in good agreement with the theoretically simulated UV spectra derived using Time-Dependent Density Functional Theory (TDDFT) calculations. Theoretical and experimental SERS are correlating well, strongly confirming the process of adsorption, the tilted orientation of naphthalene on silver surface and the adsorption mechanism reported. Localization of electron density resulting from redistribution of electrostatic potential after adsorption on silver together with the reduction in bandgap of naphthalene suggests its utility in the design of electro active organic molecular devices.

* Corresponding author. Tel.: +91 9944952925.
E-mail address: beulah_rajkumar@yahoo.co.in (B.J.M. Rajkumar).

http://dx.doi.org/10.1016/j.molstruc.2014.09.022
0022-2860/

Introduction

Aromatic hydrocarbons constitute an important class of organic compounds because of their unique properties and ubiquitous nature. The scientific interest in organic compounds adsorbed onto the metal surfaces has long been of significance, as the adsorption studies of these compounds play a vital role in establishing the modifications in their catalytic and opto-electrical properties. Adsorption of organic ligands on a metallic surface induces changes in their shape or aggregation and accounting for the effects of any surface – adsorbed molecule is crucial to understanding of behavior of metal clusters observed experimentally [1,2]. The catalyzing efficiency of the metal substrates is related to their chemical characteristics. These can be monitored by observing the vibrational behavior of the adsorbate as their vibrational modes are largely dependent on the changes in symmetry on adsorption and the orientation of the adsorbate on to the surface [3,4]. Hence the interaction mechanism of adsorbed molecules on the surface of the substrate can be analyzed based on the shift of Raman Bands and the changes in their intensity [5,6]. Raman scattering cross sections can be greatly enhanced when the analyte molecule is adsorbed on metallic surfaces and in particular on silver nanoparticles [7,8]. The adsorption of aromatic compounds onto Ag NPs has been investigated extensively in the recent years due to their useful physical and chemical properties as the substrates for Surface Enhanced Raman Spectroscopy (SERS) applications in optoelectronics and biomedical science [9].

Structural properties of several biological systems are greatly influenced by their interaction with aromatic compounds [10]. The nature of metal – molecule adsorption and the subsequent electronic structure of the molecules reveal critical factors that determine their conductivity [11,12]. Research focusing on the interactions of aromatic compounds with metals is gaining momentum recently because of their potential applications in the design of devices based on electro active organic molecules and their promising role in molecular electronics [13–15]. Naphthalene is the simplest Polycyclic Aromatic Hydrocarbon (PAH) with a fused pair of benzene rings. Although the reactions involving naphthalene have been reported to be less aromatic in nature, they have been proved to be more reactive than benzene. Naphthalene is of recent scientific interest because of its extensive industrial applications. It is widely used as a precursor for many other chemicals and in the industrial production of several synthetic dyes. It finds application in the manufacture of plastics, resins, fuels, and insecticides and is used in the synthesis of photo multiplier tubes, synthetic resins, coatings, tanning agents and celluloids. Naphthalene and its derivatives are also biologically and pharmaceutically useful compounds [16,17].

Quantum Mechanical Modeling methods are among the most efficient tools of investigations of the adsorption characteristics of nano structured systems and are useful in predicting and interpreting the characteristics of their theoretical vibrational spectra [18]. Density Functional Theory (DFT) is an efficient Quantum Mechanical Modeling approach in analyzing the molecular structures, energies and vibrational frequencies using theoretical computations. DFT has also been reported to provide excellent vibrational frequencies of organic compounds if the computed frequencies are scaled to compensate for the electron correlation; basis set deficiencies and anharmonicity [19]. Surface Enhanced Raman Spectroscopy (SERS) is a powerful technique for studying the adsorption behavior of the molecules on the substrates and for identifying the molecular orientation and interaction mechanism of the molecules with the surface of the substrate. Enhancement of selective vibrational modes and band shifts observed in SERS are explained in terms of the charge-transfer model and are sensitive to the orientation of the molecules with respect to the surface [9].

The efficient fabrication of transition metal nanoparticles is of particular importance because of their unique properties and fascinating applications in optoelectronics and biomedical science. The synthesis of metal nanoparticles especially silver, based on solution combustion method is an already established method to prepare nanosized metal particles as it involves a high level of molecular mixing of the components resulting in higher chemical homogeneity of the synthesized products with high purity in a rapid and comparatively less expensive operation. Geetha et al. had presented an SERS spectral analysis of 1,4-dibromonaphthalene (1,4-DBrN) on silver surface [9]. Prabhu et al. had carried out a spectroscopic (FTIR and FT Raman) analysis and vibrational study on 2,3-dimethyl naphthalene using HF and DFT calculations [16]. Arivazhagan et al. had recorded the solid phase FTIR and FT-Raman spectra of 1,5-dinitronaphthalene and the findings were further interpreted based on computational methods using DFT [17]. Tsikritzis et al. had investigated the electronic and interfacial properties of naphthalene bisimide derivatives on gold using photoelectron spectroscopic techniques [20]. Schnockelborg et al. had studied the electronic structures of low-valent naphthalene and anthracene iron complexes using X-ray, spectroscopic and DFT methods [21]. In the current work, adsorption of naphthalene on silver is investigated using DFT methods and SERS.

Computational methods

In the present investigation, adsorption of naphthalene on silver is studied to analyze and understand the optimized geometries, charge transfers and vibrational modes using the commercially available software package Gaussian 03 [22]. The simulated spectrum is then compared with experimental observations. This model of study can be effective in estimating the changes in energetics, structural and electronic characteristics of metal cluster systems induced by the adsorption of polycyclic aromatic hydrocarbons. Computational study was carried out at the Density Functional Theory (DFT) level using B3PW91 functional and LANL2DZ basis set. LANL2DZ basis set uses an effective core for heavier atoms and is an established standard choice for the theoretical methods involving transition metals and organometallic complexes [23–27]. Silver cluster, Ag_3, identified to be stable and reactive has been considered in this study for the theoretical analysis of adsorption characteristics. To identify the theoretical configuration on adsorption, computations were performed using identical functional and basis set for multiple initial orientations. Irrespective of the initial geometry orientations of naphthalene and silver, the adsorption geometry was the one with the naphthalene in a tilted orientation with respect to the silver cluster. All optimized geometries were derived without imposing any symmetry constraints. Convergence of all the calculations together with the absence of imaginary vibrational frequencies confirms the attainment of a local minimum on the potential energy surface [28–31]. Time-Dependent Density Functional Theory (TDDFT) computations are employed to derive the optical absorption spectral values and the corresponding theoretical absorption spectra were simulated using the SWizard program [32].

Experimental methods

Synthesis

Silver nitrate and Glycine were purchased from MERCK and were used in experiments as purchased without further purification. All

glasswares were properly washed with distilled water and dried in hot air oven before use. Silver nanoparticles were prepared by solution–combustion method using silver nitrate ($AgNO_3$) and glycine ($C_2H_5NO_2$) as oxidizer and fuel respectively [9]. $AgNO_3$ and $C_2H_5NO_2$ were mixed in 1:0.5 ratios and dissolved in 25 ml of deionised water in a crucible. For the precise and uniform formation of the desired composition on the nanoscale, this mixture was then stirred on a magnetic stirrer for about 30 min. Uniform aqueous solution was formed and this was subsequently placed on a hot plate at 300 °C. On reaching the point of spontaneous combustion, the solution began to burn, vaporizing the entire solution instantly and the combustion reaction was completed in about 20 min. A loose grayish black colored powder was formed which was crushed and ground thoroughly to obtain the silver nanoparticles (Ag NPs).

Characterization

X-ray diffraction (XRD) patterns of Ag NPs were recorded on PANalytical X-ray diffractometer using Cu Ka radiation (λ = 1.5406 Å) operated at 50 kV and 100 mA and the measurements were taken for the diffraction angle range of 2θ = 20–80°. Transmission electron microscope (TEM) images were obtained using a JEOL JEM 2100 High Resolution Transmission Electron Microscope, operating at 200 kV. The optical absorption measurements were carried out using Shimadzu UV-1700 pharmaspec UV–visible spectrophotometer. Raman spectra were recorded by micro Raman system from Jobin Yvon LABRAM-HR with He–Ne laser with an excitation wavelength of 632 nm.

Results and discussion

Structural properties

Fig. 1 depicts the optimized structure of naphthalene before and after adsorption on a three atom silver cluster (N and N—Ag). The geometrical parameters were calculated using B3PW91 functional and LANL2DZ basis set. The optimized gas-phase geometry of naphthalene is of D_{2h} symmetry and its carbon–carbon bonds are not of the same length. The carbon–carbon bonds in naphthalene are calculated to be of 1.38 Å (C=C2, C5=C6, C10=C15 and C11=C14) and 1.42 Å (C2—C3, C3—C4, C4—C5, C6—C1, C4—C11, C14—C15 and C3—C10); after adsorption, the C—C bonds nearer to the silver cluster were significantly deformed with bondlengths measuring 1.40 Å (C5=C6) and 1.43 Å (C4—C5 and C6—C1). However, the C—H bond lengths remain unchanged after adsorption. The shortest computed C—Ag distance was 2.52 Å. Silver cluster, Ag_3 maintains the same geometry after adsorption as the original cluster, although its bond lengths undergo some changes. Bond angles of naphthalene nearer to the Ag atoms were computed to be 118° (C1—C6—C5) and 119° (C2—C1—C6) with the corresponding dihedral angles at 173° (C2—C1—C6—H13) and 175° (C1—C6—C5—H12). These bond angles and dihedral angle values clearly indicate that the regular hexagonal structure of the ring nearer the Ag cluster is distorted on adsorption and there are deviations in the co-planarity of the corresponding carbon atoms which can be correlated to the chemical interactions resulting from adsorption.

Electronic properties: HOMO& LUMO, molecular electrostatic potential

The HOMO and LUMO energies are indicative of the ability of the molecule under consideration to donate or accept an electron respectively [33]. The difference in energies of HOMO and LUMO, the band gap, serves as a measure of excitability. Visualization of HOMO and LUMO can locate the regions of possible electron concentration for these two states for a given molecular system, their distribution and the changes in their molecular orbitals on excitation. Analyzing the structures of molecular orbitals in the ground state and the excited state can help us identify the binding sites of specific electrophilic and nucleophilic adsorbates. The qualitative approach of MO analysis uses a molecular orbital diagram to visualize bonding interactions in a molecule. The smaller the energy gap, the greater is the reactivity [34–39].

HOMO and LUMO of naphthalene and the naphthalene adsorbed on silver are presented in Fig. 2. HOMO of naphthalene is located mainly around the carbon atoms excluding a couple of atoms, while the LUMOs tend to form specific antibonding orbitals around the carbon atoms. However, in the case of N—Ag, the antibonding LUMOs extend to the silver cluster atoms too, whereas the HOMOs are mainly spread over a couple of Ag atoms alone and the carbon atoms of naphthalene. The shift of molecular orbitals from naphthalene to the silver atoms in the LUMO of N—Ag accounts for the intramolecular charge transfer taking place from the π to the silver. It is also interesting to note that, the band gap of naphthalene (4.82 eV) is significantly reduced after adsorption on silver (1.63 eV) and the shifting of MOs can be correlated to the transfer of charge associated with the process of adsorption.

Molecular electrostatic potential (MEP) at a given point around a molecule provides information about the net electrostatic effect at that point produced by the total charge distribution of the

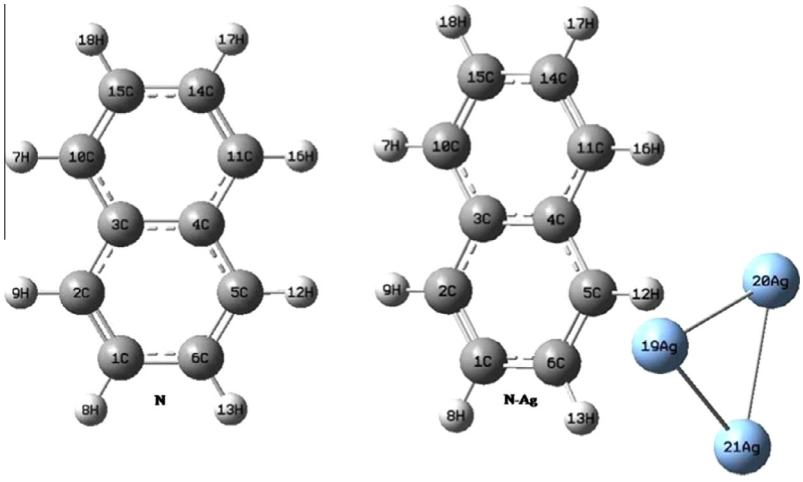

Fig. 1. Optimized geometries of naphthalene (N) and naphthalene adsorbed on silver (N—Ag).

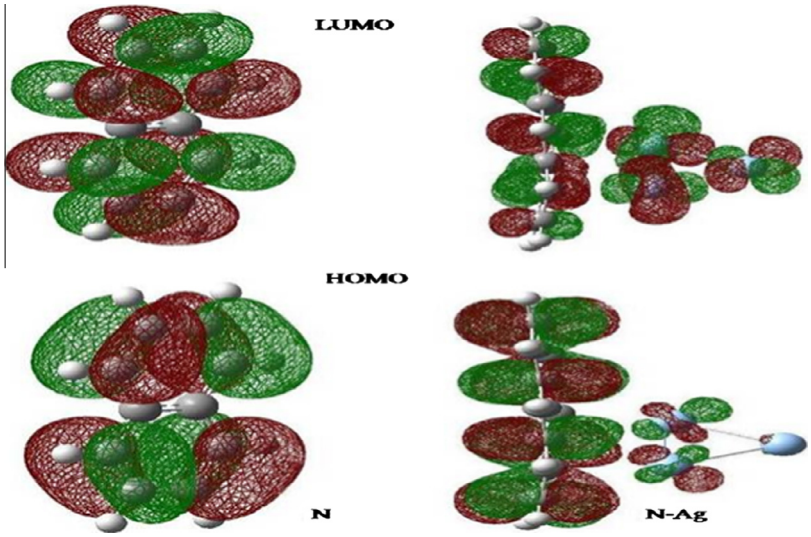

Fig. 2. Molecular orbitals.

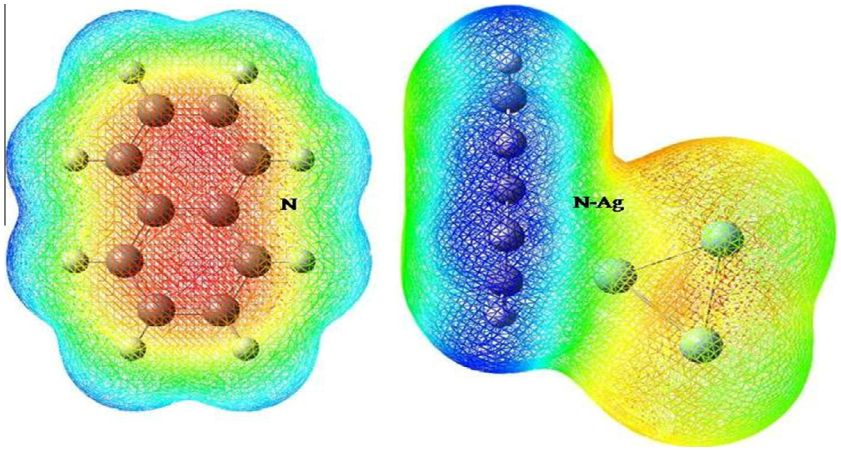

Fig. 3. Molecular electrostatic potential.

molecular system and hence can be used to predict the reactivity [33]. Visualization of the MEP surface also helps in predicting the relative polarity of the molecule [36–38]. A Map of an electron density isosurface of a molecular system with its electrostatic potential ideally depicts the shape, charge density and reactive sites of the molecules and hence can identify bonding interactions. To analyze the reactive sites and the bonding interactions, the MEP surface (electron density isosurface value 0.0004a.u.) has been plotted over the optimized geometry of the cluster systems (Fig. 3). Variations in the [1]electrostatic potential at the surface are represented by different colors, red representing regions of most negative electrostatic potential; blue the regions of most positive electrostatic potential and green representing areas of zero potential. The increase in electrostatic potential of the surface is represented in the order, red < orange < yellow < green < blue [37,40].

The carbon atoms belong to the regions of equal negative electrostatic potential and the hydrogen atoms are in the regions of equal positive potential in naphthalene. Adsorption results in regions of higher electrostatic positive potential around the ring and negative potentials around Ag atoms. Redistribution of electron density of naphthalene when adsorbed on silver is possibly due to the interactions between the delocalized π electrons of naphthalene and the valence electrons of silver, as is evident from the shifting of MOs from naphthalene to the silver atoms. Theoretically derived polarization value of naphthalene (100.72a.u) is also identified to be much higher after adsorption on silver (296.65a.u) confirming the transfer of charges from naphthalene to silver. Enhancement of polarization on adsorption resulting from the redistribution of electrostatic potential combined with a reduced bandgap can lead to applications in molecular electronics.

Natural bond orbital analysis

Natural bond orbital analysis is an effective tool for the interpretation of intra and intermolecular interactions and provides a better understanding of charge transfer from the filled to the unfilled molecular orbitals or conjugative interactions in the molecular systems [34]. Delocalization of electron density between occupied NBOs and unoccupied NBOs corresponds to a stabilizing donor–acceptor interaction and can be quantitatively described in terms of the second order perturbation interaction energy, E(2) [30,31]. The larger the value of E(2), the greater is the interaction between the electron donors and electron acceptors, and higher is the extent of conjugation of the whole system [34–36,41].

[1] For interpretation of color in Fig. 3, the reader is referred to the web version of this article.

Second order perturbation interaction energy of a molecular system can be calculated as:

$$E(2) = \Delta E_{ij} = q_i \frac{F^2_{(i,j)}}{E_j - E_i}$$

where q_i is the orbital occupancy of the ith donor, E_j and E_i are the diagonal elements (orbital energies) and $F(i,j)$ is the off diagonal NBO Fock matrix element.

The theoretically computed NBO values (Table 1) along with the higher $E(2)$ values indicate that the intramolecular interactions of naphthalene is due to the orbital overlap between π(C—C) and π^*(C—C) orbitals resulting in higher intramolecular charge transfer (ICT) along with an increase in electron density causing the stabilization of the system. In the case of N—Ag, the intramolecular interactions are identified from the overlap of the orbitals of π(C—C) to π^*(C—C) and π(C—C) to σ^*(Ag—Ag). Shift in electron density from the π(C—C) of naphthalene to the σ^* orbitals of Ag atoms accounts for higher intramolecular charge transfer on adsorption and is on expected lines as is confirmed by the shifting of MOs and the enhancement in polarization on adsorption. These intramolecular interactions can be correlated to the plot of MEP as a clear enhancement in electron density is noticed around the ring after adsorption.

XRD studies

The X-ray diffraction pattern of Ag NPs synthesized using solution–combustion method were compared and interpreted with the reflection peak characteristics of metallic silver and the peaks observed were found to be correlating well with the different crystallographic planes. Fig. 4 shows the XRD pattern of the synthesized silver NPs, with four different peaks at $2\theta = 38.11°$, 44.30°, 64.42° and 77.41° corresponding to the Bragg's reflection from the (111), (200), (220) and (311) planes respectively of the face centered cubic structure of the synthesized silver NPs [9]. Peaks pertaining to the impurities are not detected, indicating that the silver nanoparticles are pure and crystalline in nature. Size of the silver nanoparticles was estimated based on Debye–Scherrer formula,

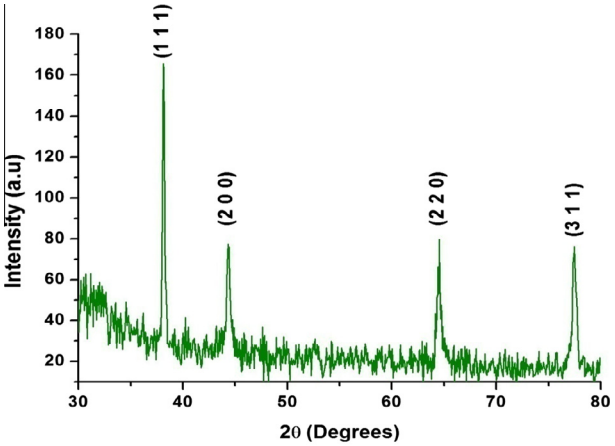

Fig. 4. X-ray diffraction pattern of silver nanoparticles.

$$D = 0.9\lambda/\beta \cos\theta$$

D is the particle size (nm), λ is the wavelength of X-ray radiation (1.5406 Å), β is the full-width at half maximum (FWHM) of the peak (in radians) and 2θ is the Bragg angle (in degrees). The calculated particle size is found to be in the range of 22 nm to 42 nm. Considering the particles to have a spherical shape, this corresponds to approximately around 11,500 atoms to a nanoparticle.

TEM analysis

The morphology and crystalline structure of the synthesized Ag NPs were further analyzed based on the images taken on High Resolution Transmission Electron Microscopy (HRTEM) and are shown in Fig. 5. TEM images indicate that the dispersed silver nanoparticles are crystalline in nature and are almost spherical in shape with the size of the particles ranging from 12 nm to 40 nm. The average particle size is 23 nm and is in accordance with the average size of the particles established in XRD. TEM images also illustrate that the Ag NPs exhibit certain amount of twinning in the crystalline

Table 1
Second order perturbation theory analysis in NBO.

	Donor NBO (i)	Acceptor NBO (j)	E(2) kcal/mol	$E(j)-E(i)$ a.u.	$F(i,j)$ a.u.
N	π C1—C2	π^* C3—C4	17.38	0.3	0.068
		π^* C5—C6	18.63	0.3	0.066
	π C3—C4	π^* C1—C2	17.56	0.28	0.066
		π^* C5—C6	17.56	0.28	0.066
		π^* C10—C15	17.56	0.28	0.066
		π^* C11—C14	17.56	0.28	0.066
	π C5—C6	π^* C1—C2	18.63	0.3	0.066
		π^* C3—C4	17.38	0.3	0.068
	π C10—C15	π^* C3—C4	17.38	0.3	0.068
		π^* C11—C14	18.63	0.3	0.066
	π C11—C14	π^* C3—C4	17.38	0.3	0.068
		π^* C10—C15	18.63	0.3	0.066
N—Ag	π C1—C2	π^* C3—C4	6.00	0.22	0.049
		π^* C5—C6	7.35	0.22	0.051
	π C3—C4	π^* C1—C2	6.21	0.23	0.05
		π^* C5—C6	7.32	0.21	0.052
		π^* C10—C15	7.29	0.22	0.052
		π^* C11—C14	6.19	0.23	0.05
	π C5—C6	π^* C1—C2	6.78	0.24	0.052
		π^* C3—C4	6.19	0.23	0.05
		σ^* Ag20—Ag21	4.67	0.21	0.042
	π C10—C15	π^* C3—C4	6.21	0.23	0.05
		π^* C11—C14	6.79	0.24	0.052
	π C11—C14	π^* C3—C4	6.02	0.22	0.049
		π^* C10—C15	7.34	0.22	0.05

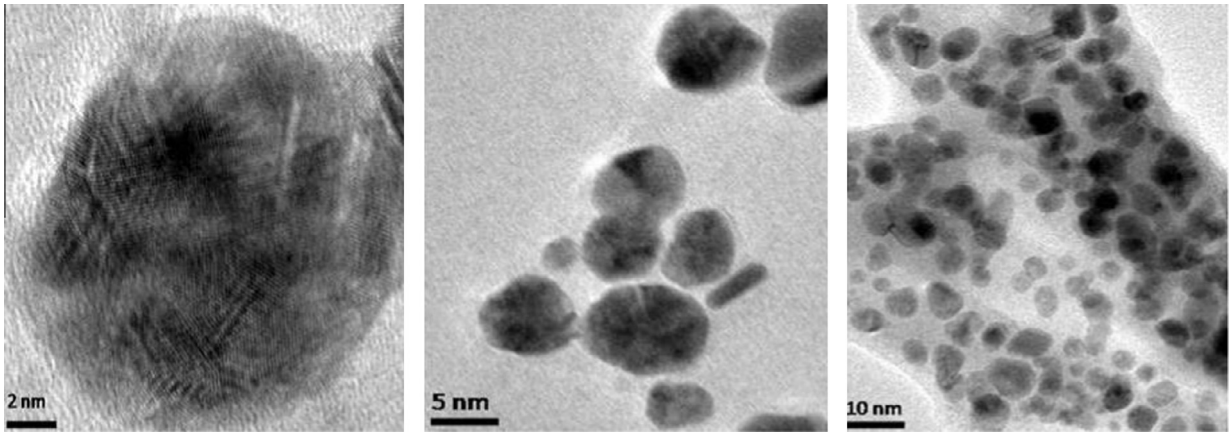

Fig. 5. TEM images of silver nanoparticles.

structure. Twinning is the planar defects in nanocrystals of face centered cubic (fcc) structure resulting from an intergrowth of two separate crystals while they share a common crystal lattice.

UV–visible spectra

Optical properties of the nanoparticles are sensitive to their size, shape, concentration and agglomeration state and hence analyzing their UV–visible spectra are crucial in studies involving identification and characterization of nanomaterials. Nanoparticles made from certain metals, such as gold and silver, strongly interact with specific wavelengths of light resulting in intense absorption peaks due to the surface plasmon excitation. This unique optical property is the foundation for the field of plasmonics. Optical properties of silver nanoparticles change when particles aggregate, the surface plasmon resonance shifts to lower energies, causing the absorption and scattering peaks to red-shift to longer wavelengths. Optical absorption spectra of N—Ag along with the theoretically simulated spectra are presented in Fig. 6. The shape of the experimental curve indicates that there is a dispersion of different sizes. It is interesting to note that the theoretical spectrum derived using naphthalene and the silver cluster Ag_3 has a good correlation with the experimental absorption spectrum of naphthalene adsorbed on silver.

Optical absorption spectrum of naphthalene adsorbed on silver has one prominent symmetric peak around 412 nm, resulting from the characteristic surface plasmon resonance of spherical silver nanoparticles and is in good agreement with the theoretically simulated UV spectra. This optical absorption band is caused by the interactions of free electrons of Ag NPs with the electromagnetic radiation incident on the surface as their electronic modes are particularly sensitive to their shape and size, resulting in pronounced effects in the visible part of the spectrum [9,42–44]. The strong narrow absorption peak confirms the spherical shape of the Ag NPs as indicated in XRD results and the TEM images. A weak secondary peak identified in the adsorption spectra can be attributed to the deviations from sphericity of the Ag NPs and the differences in distribution of the constituent atoms resulting from aggregation. Differences in intensities of theoretical absorption spectrum and that of the experimental one is mainly because the calculated spectrum is based on a single isolated N—Ag 'nanoparticle' consisting of a single naphthalene and a single Ag_3 cluster, while the measured spectrum is obtained from many N—Ag nanoparticles of approximately the same average diameter which are in each other's electrostatic environments in the solid state [31]. Further, surface plasmon resonance spectral profile would also be influenced by the variations in particle size, distribution, method of preparation and the other experimental factors like the reactants involved and the order of mixing of the reactants.

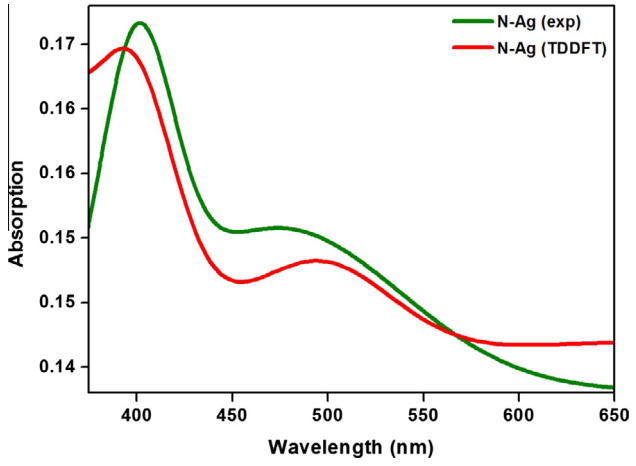

Fig. 6. Theoretical and experimental UV–Vis absorption spectrum of N—Ag.

Vibrational analysis

Variations in the vibrational modes and Raman intensities of N and N—Ag in theoretical and experimental spectra are analyzed to gain further information on the nature of naphthalene – silver adsorption (Table 2). Vibrational frequencies of naphthalene derived in this study are in good correlation with the vibrational frequencies already reported in nRS [9,45]. Theoretical values of vibrational frequencies generally differ slightly from the experimentally observed frequencies because an isolated molecule in vacuum is considered for the theoretical calculations whereas the experimental results are of large molecules in each other's electrostatic environments in the solid state.

Theoretically derived scaled Raman spectral values correlate well with the frequencies observed experimentally (Figs. 7 and 8). An intense peak noticed at 212 cm^{-1} and 232 cm^{-1} in the theoretical and experimental spectra respectively of N—Ag potentially confirms the process of adsorption as these pertain to the N—Ag vibrations and are absent in the case of naphthalene. The significant enhancement of Raman intensities is suggestive of a strong adsorption mechanism taking place between the N—Ag surfaces.

Experimental C—C in plane stretching vibrations in naphthalene has been observed at 513 cm^{-1} corresponding to the calculated peak at 507 cm^{-1}. Theses modes after adsorption are noticed in the

Table 2
Calculated (scaled) and observed Raman frequencies with assignments.

nRs (cm^{-1})		SERS (cm^{-1})		Assignments
Theoretical	Experimental	Theoretical	Experimental	
		212	232	N—Ag stretching
		459	451	Ring torsion
507	513	515	522	C—C in plane stretching
		737	737	C—H out of plane bending (asym)
		804	808	C—H out of plane bending (sym)
		890	886	C—H out of plane bending (asym)
1015	1023	999	1008	Ring stretch + C—H bending
		1108	1096	C—H in plane bending (asym)
		1130	1137	C—H in plane bending (asym)
1149	1157	1167	1163	C—H in plane bending (asym)
		1196	1185	C—H in plane bending (asym)
1236	1243	1235	1231	C—H deformation (asym)
		1265	1278	In plane ring deformation
1393	1384	1387	1382	In plane ring deformation
		1397	1405	In plane ring deformation
1617	1623	1607	1610	In plane ring deformation
1637	1649	1665	1672	In plane ring deformation

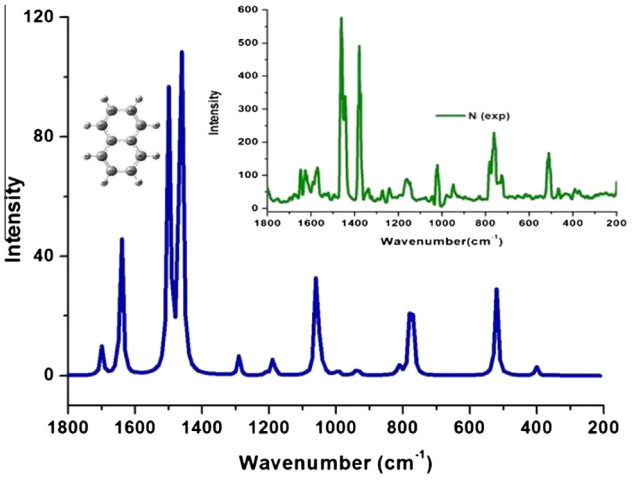

Fig. 7. Theoretical and experimental nRS of naphthalene.

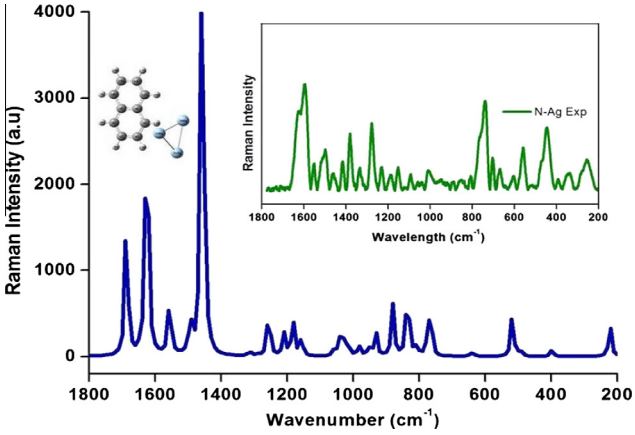

Fig. 8. Theoretical and experimental SERS of N—Ag.

experimental spectra at 522 cm^{-1} and are identified theoretically at 515 cm^{-1}, both with a considerably higher relative intensity. Naphthalene ring torsions are also identified after adsorption, theoretically at 459 cm^{-1} corresponding to an experimental peak noticed at 451 cm^{-1}. Noticeably intense additional peaks at 737 cm^{-1}, 804 cm^{-1} and 890 cm^{-1} are identified in the theoretical spectrum of N—Ag after adsorption and are associated with the out of plane C—H deformation modes arising from the bonding mechanism whereas, in naphthalene these peaks are absent further confirming that these Raman inactive modes have been excited as the symmetry of the molecule becomes lower due to the process of adsorption. Corresponding out of plane C—H deformation modes for N—Ag are observed at 737 cm^{-1}, 808 cm^{-1} and 886 cm^{-1} experimentally. The peaks at 1015 cm^{-1} and 1023 cm^{-1} in the theoretical and experimental spectra of naphthalene pertain to the asymmetric ring stretching mode and the corresponding SERS peaks are downshifted and observed at 999 cm^{-1} and 1008 cm^{-1} respectively. It is interesting to note that this mode is accompanied by a significant C—H bending also in SERS, whereas these are absent in the normal Raman spectrum of naphthalene. Further, the presence of these C—H bending modes along with the downshifting of the ring stretching modes indicates the weakening of the C=C bonds which can be considered as a direct consequence of the charge transfers resulting from adsorption as indicated by the NBO analysis.

SERS have also revealed additional intense peaks on adsorption at 1096 cm^{-1}, 1137 cm^{-1} and 1185 cm^{-1} pertaining to the C—H in plane deformation vibrations, corresponding to the peaks noted at 1108 cm^{-1}, 1130 cm^{-1} and 1196 cm^{-1} theoretically, that are relatively much higher in intensity. It is also interesting to note that these peaks are absent in the spectra of naphthalene. The presence of these vibrations along with the enhancement in intensity strongly confirms the process of adsorption. Ring deformation vibrations of naphthalene are observed at 1384 cm^{-1}, 1623 cm^{-1} and 1649 cm^{-1} corresponding to the theoretical peaks identified at 1393 cm^{-1}, 1617 cm^{-1} and 1637 cm^{-1}. Whereas these vibrational modes are observed with much higher intensity in SERS of N—Ag experimentally at 1278 cm^{-1} 1382 cm^{-1} 1405 cm^{-1} 1610 cm^{-1} and 1672 cm^{-1} corresponding to the respective theoretical peaks at 1265 cm^{-1}, 1387 cm^{-1}, 1397 cm^{-1}, 1607 cm^{-1} and 1665 cm^{-1}.

Adsorption orientation of organic moieties on the metal surfaces can be inferred based on shifts and enhancements in ring stretching vibrations, in plane and out of plane C—H bending vibrations and SERS selection rules [9,31]. It has been documented that the ring stretching modes would be red shifted on adsorption of organic moieties on metal surfaces, if the adsorption interaction is between the π orbitals of the ring and the valence orbitals of the metal involved. This is established in our investigations also, correlating well with the theoretically inferred charge transfers. Further, the presence of intense out of plane C—H bending modes in SERS suggests a strong adsorption interaction of naphthalene

on silver. Additionally, enhancements identified for in plane C—H bending vibrational modes in the theoretical and experimental SERS imply a certain angle between the ring and the silver surface, further indicating a tilted orientation of the adsorbate on the surface [31]. Significant enhancement in intensities of these vibrational modes together with the red shifting of the ring stretching mode validate that the interactions between the ring and silver nanoparticles are very strong and confirm the tilted orientation of naphthalene on silver surface.

It is also interesting to note that the theoretically calculated polarizability values of the molecular system of naphthalene adsorbed on silver are much higher after adsorption (353a.u) as compared to that of naphthalene (55a.u). This increase in polarization can be attributed to the charge transfers associated with the process of adsorption.

Conclusions

Structural and spectroscopic properties of naphthalene adsorbed on silver are studied using methods based on DFT and SERS. Adsorption of naphthalene on silver results in distortion of hexagonal structure of the ring along with significant deviations in co-planarity of carbon atoms in the optimized geometry. Binding interactions through π electrons is established theoretically confirming intramolecular charge transfer from naphthalene to silver after adsorption. Silver nanoparticles were synthesized by solution combustion method. Morphology and the crystalline nature of Ag NPs were confirmed by XRD studies and HRTEM analysis. Intense out of plane and in plane C—H deformation vibrations identified in SERS along with the downshifting of the ring stretching modes strongly confirm the process of adsorption and infer the tilted orientation of naphthalene on silver surface. Enhancement in polarization values on adsorption and the charge transfers identified theoretically from NBO analysis validate adsorption characteristics reported. Significant reduction identified in the band gap of naphthalene after adsorption on silver and the enhancement of polarization from the redistribution of electron density can further explore their potential roles in the design of devices based on electro active organic molecules.

Acknowledgements

The author M. Umadevi is thankful to DST-SERB, New Delhi and UGC-DAE-CSR, Indore for financial assistance.

References

[1] S. Goel, K.A. Velizhanin, A. Piryatinski, S. Tretiak, S.A. Ivanov, J. Phys. Chem. Lett. (2010) 927–931.
[2] V. Arcisauskaite, J. Kongsted, T. Hansen, K. Mikkelsen, Chem. Phys. Lett. 470 (2009) 285–288.
[3] W. Ma, Y. Fang, J. Colloid Interf. Sci. 303 (2006) 1–3.
[4] C. Jing, Y. Fang, Chem. Phys. 332 (2007) 27–32.
[5] Z. Tao, Y. Fang, J. Mol. Struct. 797 (2006) 40–43.
[6] J. Choudhury, J. Sarkar, R. De, M. Ghosh, G.B. Talapatra, Chem. Phys. 330 (2006) 172–183.
[7] X. Zhao, Y. Fang, B. Yan, H. Gao, J. Mol. Struct. 998 (2011) 49–52.
[8] L. Zhao, L. Jensen, G.C. Schatz, J. Am. Chem. Soc. 128 (2006) 2911–2919.
[9] K. Geetha, M. Umadevi, G.V. Sathe, R. Erenler, Acta, Part A 116 (2013) 236–241.
[10] L.M. Woods, S.C. Badescu, T.L. Reinecke, Phys. Rev. [Sect.] B 75 (2007) 155415.
[11] V. Chis, M.M. Venter, N. Leopold, Vib. Spectrosc. 48 (2008) 210–214.
[12] J.P. Jalkanen, F. Zerbetto, J. Phys. Chem. B 110 (2006) 5595–5601.
[13] J. Granatier, M. Dubecky, P. Lazar, M. Otyepka, P. Hobza, J. Chem. Theory Comput. 9 (2013) 1461–1468.
[14] S. Li, V.R. Cooper, T. Thonhauser, A. Puzder, D.C. Langreth, J. Phys. Chem. A 112 (2008) 9031–9036.
[15] W. Liu, J. Carrasco, B. Santra, A. Michaelides, M. Scheffler, A. Tkatchenko, New J. Phys. 15 (2013) (2012) 053046.
[16] T. Prabhu, S. Periandy, S. Mohan, Spectrochim. Acta, Part A 78 (2011) 566–574.
[17] M. Arivazhagan, V. Krishnakumar, R.J. Xavier, G. Ilango, V. Balachandran, Acta, Part A 72 (2009) 941–946.
[18] A.M. Tolmachev, D.A. Firsov, T.A. Kuznetsova, K.M. Anuchin, Prot. Metal. Phys. Chem. Surf. 45 (2) (2009) 177–183.
[19] G.D. Fleming, I. Golsio, A. Aracena, F. Celis, L. Vera, R. Koch, M.C. Vallette, Spectrochim. Acta, Part A 71 (2008) 1049–1055.
[20] D. Tsikritzis, P. Gawrys, M. Zagorska, S. Kennou, Microelectron. Eng. 112 (2013) 174–178.
[21] E. Schnockelborg, M.M. Khusniyarov, B. Bruin, F. Hartl, T. Langer, M. Eul, S. Schulz, R. Pottgen, R. Wolf, dx.doi.org/10.1021/ic300366m.
[22] M.J. Frisch, G.W. Trucks, H.B. Schlegel, G.E. Scuseria, M.A. Robb, J.R. Cheeseman, J.A. Montgomery Jr., T. Vreven, K.N. Kudin, J.C. Burant, J.M. Millam, S.S. Iyengar, J. Tomasi, V. Barone, B. Mennucci, M. Cossi, G. Scalmani, N. Rega, G.A. Petersson, H. Nakatsuji, M. Hada, M. Ehara, K. Toyota, R. Fukuda, J. Hasegawa, M. Ishida, T. Nakajima, Y. Honda, O. Kitao, H. Nakai, M. Klene, X. Li, J.E. Knox, H.P. Hratchian, J.B. Cross, C. Adamo, J. Jaramillo, R. Gomperts, R.E. Stratmann, O. Yazyev, A.J. Austin, R. Cammi, C. Pomelli, J.W. Ochterski, P.Y. Ayala, K. Morokuma, G.A. Voth, P. Salvador, J.J. Dannenberg, V.G. Zakrzewski, S. Dapprich, A.D. Daniels, M.C. Strain, O. Farkas, D.K. Malick, A.D. Rabuck, K. Raghavachari, J.B. Foresman, J.V. Ortiz, Q. Cui, A.G. Baboul, S. Clifford, J. Cioslowski, B. Stefanov, B.G. Liu, A. Liashenko, P. Piskorz, I. Komaromi, R.L. Martin, D.J. Fox, T. Keith, M.A. Al-Laham, C.Y. Peng, A. anayakkara, M. Challacombe, P.M.W. Gill, B. Johnson, W. Chen, M.W. Wong, C. Gonzalez, J.A. Pople, Gaussian 03, Revision B.03; Gaussian Inc.,Pittsburgh, PA, 2003.
[23] S.M. Tekarli, M.L. Drummond, T.G. Williams, T.R. Cundari, A.K. Wilson, J. Phys. Chem. A 113 (2009) 8607–8614.
[24] S.L. Poornima, M.S. Rohini, K.M. Nalin, J. Mol. Struct. 639 (2003) 195–201.
[25] Y. Yue, N.W. Michael, M.M. Kenneth, J. Phys. Chem. A 113 (2009) 9843–9851.
[26] M. Davor, E. Mirjana, Chemistry 30 (2006) 1149–1154.
[27] D.S. Samuel, D. Laurent, K. Brice, T. Thierry, O. Celine, Chem. Eur. J. 20 (2014) 7017–7024.
[28] J. Zhou, Z.H. Li, W. Wang, K.N. Fan, J. Phys. Chem. A 110 (2006) 7167–7172.
[29] S. Zhao, Y. Ren, Y. Ren, J. Wang, W. Yin, J. Phys. Chem. A 114 (2010) 4917–4923.
[30] L. Cheng, K.X. Yu, L.Z. Wen, M. Jie, M.Y. Ming, J. Phys. Chem. A 115 (2011) 9273–9281.
[31] D. Sajan, V.B. Jothy, T. Kuruvilla, I.H. Joe, J. Chem. Sci. 122 (4) (2010) 511–519.
[32] S.I. Gorelsky, SWizard program, revision 2.0, <http://www.sg-chem.net/>.
[33] T. Karthick, V. Balachandran, S. Perumal, A. Nataraj, J. Mol. Struct. 1005 (2011) 202–213.
[34] M. Arivazhagan, R. Kavitha, J. Mol. Struct. 1011 (2012) 111–120.
[35] M. Govindarajan, M. Karabacak, A. Suvitha, S. Periandy, Acta, Part A 89 (2012) 137–148.
[36] V. Balachandran, A. Lakshmi, A. Janaki, J. Mol. Struct. 1006 (2011) 395–401.
[37] R. Gayathri, M. Arivazhagan, Spectrochim. Acta, Part A 81 (2011) 242–250.
[38] V. Krishnakumar, D. Barathi, R. Mathammal, Spectrochim. Acta, Part A 86 (2012) 196–204.
[39] V. Krishnakumar, K. Murugeswari, N. Prabavathi, R. Mathammal, Spectrochim. Acta, Part A 91 (2012) 1–10.
[40] M. Karabacak, M. Cinar, M. Kurt, A. Poiyamozhi, N. Sundaraganesan, Spectrochim. Acta, Part A 117 (2014) 234–244.
[41] A. Suvitha, S. Periandy, S. Boomadevi, M. Govindarajan, Spectrochim. Acta, Part A 117 (2014) 216–224.
[42] Y. Sun, K. Balasubramanian, T.U. Rao, T. Pradeep, J. Phys. Chem. C 115 (2011) 20380–20387.
[43] E. Saion, E. Gharibshahi, K. Naghavi, Int. J. Mol. Sci. 14 (2013) 7880–7896.
[44] S. He, J. Yao, P. Jiang, D. Shi, H. Zhang, S. Xie, S. Pang, H. Gao, Langmuir 17 (2001) 1571–1575.
[45] M. Anuratha, A. Jawahar, M. Umadevi, V.G. Sathe, P. Vanelle, T. Terme, V. Meenakumari, A.F.B. Milton, Spectrochim. Acta Part A 105 (2013) 218–222.